

# CONSTRAINTS ON FUNDAMENTAL COSMOLOGICAL PARAMETERS WITH UPCOMING EPOCH OF REIONIZATION OBSERVATIONS

JUDD D. BOWMAN<sup>1</sup>, MIGUEL F. MORALES<sup>2</sup>, JACQUELINE N. HEWITT<sup>1</sup>

*Draft version January 12, 2019*

## ABSTRACT

The first generation of epoch of reionization experiments have the potential to characterize the processes and history of reionization for redshifts  $6 < z < 12$  by observing the power spectrum of the redshifted 21 cm radiation. These power spectrum observations could also contribute to our knowledge of the underlying cosmology, particularly at redshifts before the effects of reionization strongly dominate the cosmic radio background. In this paper we explore the cosmological constraints of 21 cm power spectrum observations with the Mileura Widefield Array (MWA) and its potential successor, the MWA5000, assuming a flat  $\Lambda$ CDM cosmology and that reionization occurs below a redshift of  $z = 8$ . In addition to a standard set of cosmological parameters, we include two nuisance parameters related to the systematics and foregrounds faced by radio observations. While the MWA observations cannot constrain the underlying cosmology, MWA5000 could provide useful constraints, in particular on the slope of the inflationary power spectrum,  $n_s$ , and the running of the spectral index,  $s_r$ .

*Subject headings:* Cosmology: Early Universe, Galaxies: Intergalactic Medium, Radio Lines: General, Techniques: Interferometric

## 1. INTRODUCTION

Observations of highly redshifted 21 cm neutral hydrogen emission from the epoch of reionization (EOR) and earlier will provide unique new probes of inflationary cosmology, galaxy and structure formation, and the first luminous objects. Density fluctuations in the neutral hydrogen are revealed directly in the brightness temperature of the redshifted 21 cm neutral hydrogen line (Sunyaev & Zeldovich 1972; Hogan & Rees 1979; Scott & Rees 1990; Shapiro et al. 1994; Loeb & Zaldarriaga 2004; Barkana & Loeb 2005b). Statistical measurements of the neutral hydrogen power spectrum (Morales & Hewitt 2004; Zaldarriaga et al. 2004; Bharadwaj & Ali 2005) offer the most cosmological power, and may be achieved by the first generation of low-frequency radio arrays (Bowman et al. 2006).

In this paper, we expand on earlier calculations of the sensitivity of low-frequency arrays to the 21 cm neutral hydrogen power spectrum to estimate the ability of such experiments to constrain cosmological models. These studies build on a body of work in how to use 21 cm observations to study cosmology (Barkana & Loeb 2005a; Ali et al. 2005; Barkana 2006), and in parameter estimation from cosmic microwave background (CMB) anisotropy experiments (Knox 1995; Jungman et al. 1996; Zaldarriaga et al. 1997; Bond et al. 1997; Verde et al. 2003; Spergel et al. 2003) and from large-scale structure measurements with galaxy redshift surveys (Feldman et al. 1994; Tegmark et al. 1998; Percival et al. 2001; Hu & Haiman 2003; Tegmark et al. 2004a,b; Cole et al. 2005).

Using the 21 cm neutral hydrogen power spectrum would provide an independent method to test cosmological models at an intermediate redshift and may help to remove existing degeneracies between model parameters. As an initial effort, we forecast constraints for upcoming experiments designed to

measure the neutral hydrogen power spectrum below redshift  $z < 12$ . We neglect the effects of redshift distortions and assume that reionization has not occurred at the target redshifts of  $8 < z < 10$ . The forecasted constraints are described in terms of statistical errors using a Fisher matrix treatment of the full three-dimensional power spectrum which marginalizes over several cosmological parameters and two anticipated additional contributions related to astrophysical foregrounds. The results are encapsulated in Figure 2.

A similar analysis has been performed in parallel by McQuinn et al. (2006). While we focus on the ability of just the EOR experiments to study cosmology and explore the underlying behavior of the constraints in the presence of residual foreground contaminants, they discuss these experiments in combination with information from other experiments, such as WMAP and Planck. The approaches are complimentary, with similar results, and together provide a thorough analysis of the potential of future EOR experiments as probes of cosmology.

We begin in Section 2 by reviewing the observational process of measuring the highly redshifted 21 cm neutral hydrogen power spectrum. In Section 3, we differentiate three contributions to the measured power spectrum and establish the model used for calculating constraints on cosmological parameters. In Section 4 we show the results of the analysis and discuss significant findings.

## 2. THE MEASUREMENT

Neutral hydrogen is optically thin to the 21 cm line, thus the visibility measurements of low-frequency radio arrays inherently sample the emission from a three-dimensional volume of space at high redshift. By applying a Fourier transform along the line-of-sight direction, the measurements may be represented as a cylinder in a fully Fourier domain and expressed in coordinates convenient for studying cosmology ( $\mathbf{k} = k_1; k_2; k_3$ ) or in coordinates more directly related to instrumental considerations ( $u; v; \ell$ ).

The 21 cm power spectrum is mapped to an instrumental response by the convolution of the power spectrum,  $P_{HI}$ ,

arXiv:astro-ph/0512262v1 12 Dec 2005

<sup>1</sup> MIT Kavli Institute for Astrophysics and Space Research, 77 Massachusetts Avenue, Cambridge, MA 02139, USA

<sup>2</sup> Harvard-Smithsonian Center for Astrophysics, 60 Garden Street, Cambridge, MA 02138, USA  
Electronic address: jdbowman@mit.edu

with the instrumental window function,  $W(\mathbf{k})$ , according to (Morales & Hewitt 2004)

$$C^{HI}(\mathbf{k}) = \int I(\mathbf{k})^2 = P_{HI}(\mathbf{k}) \int W(\mathbf{k}-\mathbf{k}^0) d^3k^0 \quad (1)$$

The window function is given by the Fourier transform of an array's spatial and frequency response and is very sharply peaked for the experiments we will consider.

There is an inherent uncertainty to the power spectrum measurement from cosmic sample variance. The uncertainty can be estimated by dividing the Fourier space into a large number of independent cells, where the volume of each cell is approximately the size of the window function,  $W(\mathbf{k})$ . The cosmic sample variance is related the number of independent cells in the measurement.

### 2.1. Contributions from Astrophysical Foregrounds

The 21 cm emission is not the only source of power in low-frequency radio observations. Astrophysical foregrounds are several orders of magnitude stronger and dominate the measured signal. The foregrounds include free-free and synchrotron emission from the Galaxy, extragalactic point sources, and free-free emission from elections in the intergalactic medium (Di Matteo et al. 2004).

The bright foregrounds manifest themselves in several ways. First, the Galactic emission dominates the thermal noise in the measurements, especially at lower frequencies. Although much of this large-scale emission is expected to be resolved-out by interferometric observations, its effect on antenna temperature remains.

The contribution to the measured power spectrum due to thermal noise is substantial, but white ( $C^N = const$ ), and therefore should be readily removed. The remaining thermal uncertainty per independent cell can be approximated, in instrumental coordinates, using (Morales 2005, His Equation 11)

$$C_{ij}^N(\mathbf{u})_{rms} = 2 \frac{2k_B T_{sys}}{dA d}^2 \frac{1}{B n(\mathbf{u}) t} \quad (2)$$

where  $dA$  is the physical antenna area,  $d$  is the inverse of the total bandwidth,  $k_B$  is Boltzmann's constant,  $T_{sys}$  is the total system temperature,  $\eta$  is the efficiency,  $B$  is the total bandwidth,  $\bar{n}$  is the time average number of baselines in an observing cell, and  $t$  is the total observation time. The thermal uncertainty is approximately independent of frequency within the observing band. Additionally, for the arrays we will consider, the visibility distributions are expected to have approximately circular symmetry.

The second important effect of astrophysical foregrounds is that they produce their own signatures in the measured power spectrum. Recent studies indicate that statistical techniques should provide methods to separate the foregrounds from the 21 cm neutral hydrogen power spectrum (Morales et al. 2006; Zaldarriaga et al. 2004; Morales & Hewitt 2004; Santos et al. 2005; Wang et al. 2006).

Let us assume that the foregrounds have been cleaned from the measured signal. Even the best subtraction algorithms leave residual traces of the contaminate, however, and a perfect model may produce an imperfect subtraction simply due to thermal uncertainty in the measurement. Such a subtraction error would result in a power spectrum signature following the shapes of the model components (Morales et al. 2006). For astrophysical foreground emission which can be modeled by a low-order polynomial in frequency, such as extragalactic

point sources, the principle residual signature for this kind of subtraction error can be quantified as a  $k_3$ -dependent factor,  $C^F(k_3) / k_3^{-2}$ . Since extragalactic sources are expected to be the most significant astrophysical foreground contaminate we include this contribution in our analysis.

### 2.2. Reference Experiments

We have chosen two reference experiments for the analysis in this paper. The first is based on the fiducial observation described in Bowman et al. (2006, Their Section 2) for the planned Mileura Widefield Array (MWA). The MWA array design consists of 500 antennas distributed within a 1500 m diameter circle. The density of antennas as a function of radius is taken to go as  $r^{-2}$ , but capped at a maximum density of one antenna per 16 m<sup>2</sup>. The field of view is 15-45°, depending on frequency, and the bandwidth is 32 MHz.

The second reference experiment is based on an expanded MWA configuration similar to the one considered by Wyithe et al. (2006), although more condensed, dubbed MWA5000. Here, the array is expanded to 5000 antennas distributed over a 3000 m diameter region. The density of antennas remains  $r^{-2}$  and capped at one per 16 m<sup>2</sup>. The field of view and bandwidth are also unchanged. In both experiments all antenna elements are correlated to preserve the large field of view.

For the analysis in this paper, we define the observation to be of a single field with 1000 hours integration during the most favorable circumstances. Additionally, we set the frequency coverage to  $125 < f < 157$  MHz, which spans  $8 < z < 10$ , and treat the bandwidth as four consecutive 8 MHz regions, each of which spans approximately  $z = 0.5$ . In principle, the observed 21 cm power spectrum is varying continuously with redshift due to cosmology-dependent effects. By dividing our measured volume of space into thin regions in redshift we may ignore cosmic evolution within each region without substantial loss of information over all and without detrimental effects to the derived cosmological constraints.

### 3. THE MODEL

The Fisher matrix formalism we use to study constraints on cosmological models depends on a good parametrization of its space of models. We use a parametrization based on three contributions:

$$P(\mathbf{k}) = P_{HI}(k) + P_F(k_3) + P_N; \quad (3)$$

where the first term is the neutral hydrogen contribution, the second is the predicted residual astrophysical foreground contribution discussed in Section 2.1, and the third is the residual offset after subtraction of the white thermal noise power spectrum.

The neutral hydrogen contribution, assuming no reionization has occurred, is

$$P_{HI}(k) = C_{Jy}^2 P(k; \mathcal{A}; M; b; h; n_s; s); \quad (4)$$

where  $C_{Jy}$  is the strength of the 21 cm emission from neutral mean density gas and  $P(\mathbf{k})$  is the matter power spectrum at a given redshift. The parameters we use to describe the matter power spectrum are given in Table 1 along with their fiducial values. Additionally, we constrain  $\kappa = 0$  and  $\beta = 1 - M$ .

As described in Section 2.1, the predicted residual foreground contribution is expressed as

$$P_F(k_3) = c_{norm} F \frac{k_3^{-2}}{0.01 \text{Mpc}^{-1}}; \quad (5)$$

TABLE 1  
MODEL POWER SPECTRUM PARAMETRIZATION

Parameter	Symbol	Fiducial Value
Normalization (at $k = 0.05 \text{ Mpc}^{-1}$ )	$A$	1.00
Matter density	$M$	0.30
Baryon density	$b$	0.05
Hubble constant	$h$	0.70
Scalar spectral index (at $k = 0.05 \text{ Mpc}^{-1}$ )	$n_s$	1.00
Running index slope (at $k = 0.05 \text{ Mpc}^{-1}$ )	$s$ $dn_s = d \ln k$	0.00
Residual foreground amplitude	$F$	0.00
Residual thermal offset	$N$	0.00

NOTE. — Eight parameters used to describe the measured power spectrum, and their values for the fiducial model. The first six rows give the basic parameters used to describe the matter power spectrum and the last two rows give the parameters to quantify the residual astrophysical foreground and residual thermal offset terms.

where  $c_{norm}$  is a normalization constant and  $F$  is an amplitude scale factor of order unity. The residual thermal offset contribution does not vary with  $\mathbf{k}$  and is defined as  $P_N = c_{norm} N$ , where  $N$  is also an amplitude scale factor of order unity. For the Fisher matrix analysis, both  $P_F$  and  $P_N$  are normalized by setting  $c_{norm} = P_{HI}(0.01 \text{ Mpc}^{-1})$  at redshift  $z = 8$ . Thus, the magnitudes of  $F$  and  $N$  give the amplitudes of the residual contributions relative to the peak of the neutral hydrogen power spectrum. Combining  $F$  and  $N$  with the cosmological parameters gives the eight parameters,  $p = \{A; M; b; h; n_s; s; F; N\}$ , which constitute the free variables of our base model.

As stated earlier, in this paper we assume that no reionization has occurred before or during the epoch targeted by the measurements. This allows for the straightforward expression in Equation 4 and dramatically simplifies the interpretation of the results. Furthermore, we compute the matter power spectrum using CMBFAST (Seljak & Zaldarriaga 1996) and do not include velocity distortions.

### 3.1. Parameter Dependencies

To gain a conceptual understanding of the constraints shown in Figure 2, it is instructive to individually vary the cosmological parameters and compare the resulting signals. On all but the largest length scales, the experimentally observed power spectrum is well approximated by the equation

$$P_{HI}(u;v; \mathbf{k}) = W^2 C_{Jy}^2 P(\mathbf{k}) \frac{d^3 \mathbf{k}}{dudvd} ; \quad (6)$$

where  $W$  is the integrated value of the observational window function and represents the signal strength for a given observatory, and  $d^3 \mathbf{k} = dudvd$  is the Jacobian for converting the matter power spectrum ( $\text{Mpc}^3$ ) to observed units given in  $u;v; \mathbf{k}$ .

There are three separate terms which may be affected by changing cosmological parameters: 1) the neutral hydrogen emission factor  $C_{Jy}$ , 2) the matter power spectrum itself, and 3) the coordinate mapping between  $\mathbf{k}$  and  $u;v; \mathbf{k}$ . The first term is unique to EOR experiments, and the third term allows differences between the line-of-sight and transverse directions to contribute to the constraints. Unlike galaxy surveys, the amplitude of the 21 cm fluctuations can be used as a constraint.

Assuming the spin temperature of the neutral hydrogen is significantly warmer than the CMB, the hydrogen emission factor goes as (Morales & Hewitt 2004, Their Equation 13

and Their Appendix A)

$$C_{Jy} / \frac{b h^2}{h E(z)} x_{HI} ; \quad (7)$$

where  $E(z) = \frac{1}{M(1+z)^3 + k(1+z)^2 + (1+z)^{3(1+w)}}$  and  $x_{HI}$  is the mean neutral fraction (assumed to be one in this paper).

The mapping between  $\mathbf{k}$  and  $u,v$ , produces two effects when measuring the power spectrum. First, the measured power spectrum will occupy different ranges along  $u;v$  and for different cosmologies, akin to the CMB power spectrum shifting in  $l$ . A difference in the observed parallel and line-of-sight dimensions gives rise to the Alcock-Paczynski (AP) test (Alcock & Paczynski 1979). Second, since the Jacobian contributes to the amplitude of the observed power spectrum, there is a cosmology-dependent amplitude factor. The relationships between  $u;v; \mathbf{k}$  and  $\mathbf{k}$  are (Morales & Hewitt 2004):

$$[k_1; k_2] = \frac{2}{D_M(z)} [u; v] \quad (8)$$

$$k_3 = \frac{2 \cdot 21 H_0 E(z)}{c(1+z)2} ; \quad (9)$$

where  $D_M(z)$  is the transverse comoving distance and  $21$  is 1.42 GHz. By combining Equations 8 and 9 we can calculate the Jacobian

$$\frac{d^3 \mathbf{k}}{dudvd} = \frac{(2 \cdot 21 H_0 E(z))^3}{c(1+z)^2 D_M^2(z)} ; \quad (10)$$

From combining Equations 7 and 10, the amplitude of the observed power spectrum is then proportional to

$$P_{HI} / \frac{2^3 b^3 h^3}{(1+z)^2 D_M^2(z) E(z)} P ; \quad (11)$$

and we note that  $D_M(z) / h^{-1}$ .

Figure 1 shows the observed signal and measurement uncertainties for the fiducial model (thick line,  $b = 0.05$ ,  $M = 0.30$ ,  $h = 0.70$ ,  $n_s = 1.00$ ,  $s = 0$ ) along with the expected signals obtained by varying individual parameters. The effect of varying the cosmological parameters can be classified into three categories: amplitude scaling, power spectrum shape, and coordinate mapping effects.

Looking at Figure 1 we can see that varying  $b$  or  $h$  primarily results in a simple scaling of the observed power spectrum, as expected from Equation 11. Thus these parameters are highly degenerate with each other and with the amplitude factor  $A$ , as shown in Figure 2.

The primordial power spectrum slope  $n_s$  and running of the spectral index  $s$  do not enter into the overall amplitude of the observed signal, but instead affect the shape of the underlying matter power spectrum. In Figure 1, increasing  $n_s$  lowers the power at small  $k$  and increases the power at large  $k$ , whereas increasing  $s$  boosts the power spectrum at both extremes. Because these parameters do not strongly affect the amplitude normalization, they are largely independent of  $A$ ,  $b$ , and  $h$  as shown in Figure 2. Less intuitively, they are also independent of our foreground parameter,  $F$ , because the shape they introduce is different than the  $k^{-2}$  shape of the residual foreground contamination. Thus  $n_s$  and  $s$  are the best constrained cosmological parameters for the proposed 21 cm observations.

The last class of observational effects is from the coordinate mapping. Most significantly, for an increase in  $h$ , a radially inward shift of scales (see Equations 8 and 9, with  $D_M(z) / h^{-1}$ )

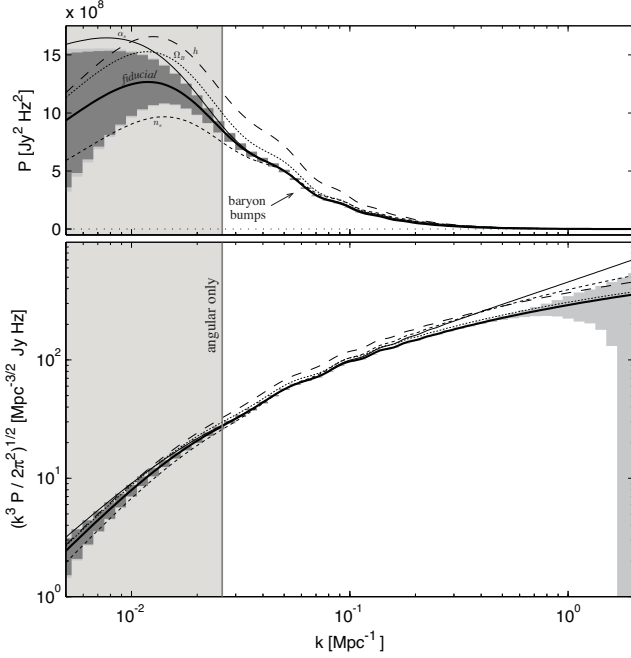


FIG. 1.— The sensitivity of MWA5000 reference experiment shown with four example variations of the cosmological model. The top panel is plotted in observers’ units where the uncertainty is Gaussian, while the lower panel shows the same elements in more common theorists’ units. The thick solid line is for the fiducial model with standard cosmological parameters ( $\Omega_b = 0.05$ ,  $\Omega_M = 0.30$ ,  $h = 0.70$ ,  $n_s = 1.00$ ,  $s = 0$ ). The other curves are produced by adjusting one cosmological parameter from the fiducial:  $\Omega_b + 10\%$  (dotted),  $h + 10\%$  (long dash),  $n_s + 10\%$  (short dash), and  $s = 0.1$  (thin solid). The dark shaded region indicates the cosmic variance within the observed field and dominates at small  $k$ , while the thermal uncertainty is shown as a light region and dominates at large  $k$ . Due to the limited redshift range over which cosmic evolution can be neglected ( $\approx 8$  MHz), the measurements to the left of the vertical line are constrained only by angular fluctuations and will thus be most affected by astrophysical foreground contamination.

counteracts the amplitude increase from the  $C_{Jy}$  and Jacobian factors. Increasing  $\Omega_M$  also shifts scales inward (through  $E(z)$  and  $D_M(z)$ ), but does so differently for the line-of-sight direction and the transverse directions. This AP effect cannot be represented easily in Figure 1, however, we have included it in all the constraints. The significance of the effect is limited since we take  $\Omega_M = 1 - \Omega_b - \Omega_s$ . A 10% increase in  $\Omega_M$  yields an approximately 4% reduction in scale, but only about 1% distortion between the directions. In general, coordinate based effects may be better constrained with observations targeting the EOR since sharper spatial features in the power spectrum may emerge during reionization due to characteristic sizes of Stromgren spheres.

#### 4. RESULTS

The Fisher information matrix provides a convenient method for translating uncertainties in power spectrum measurements to constraints on cosmological parameters (Tegmark et al. 1997). The method uses a set of observables and a parameterized model to predict the observables. It yields the minimum possible errors on unbiased estimators of parameters assuming that the true values are those of a fiducial model and that all errors are gaussian. The method is an approximation that holds only for small excursions from the fiducial model. The minimum errors are calculated using the

Fisher matrix:

$$F_{ab} = \sum_i \frac{1}{\langle P_i \rangle^2} \frac{\partial P_i(\mathbf{k}_i)}{\partial p_a} \frac{\partial P_i(\mathbf{k}_i)}{\partial p_b}; \quad (12)$$

where  $\sum_i \frac{1}{\langle P_i \rangle^2} + \frac{1}{P_{HI}}$  is the combined uncertainty per independent cell in the measured power spectrum,  $P$  is the measured power per cell given by Equation 3, and  $p$  are the model parameters. Taking the square roots of the diagonal elements of the inverse of Fisher matrix gives the errors.

The results of performing the Fisher matrix calculations for the two reference experiments described above are summarized in Tables 2-4, which list the forecasted 1- $\sigma$  uncertainties on the model parameters and the elements of the covariance matrices. These values indicate that the initial MWA design, even with the optimistic assumptions that the astrophysics of reionization is negligible at the target redshifts, does not constrain the cosmological parameters significantly. The MWA5000, however, does reasonably constrain all the model parameters at levels equivalent to or better than those from the first-year WMAP results (Spergel et al. 2003, Their Table 10).

Figure 2 provides additional information about the forecasted constraints for the MWA5000. It shows marginalized error ellipses for two-parameter combinations. The plot regions have been scaled to the first-year WMAP constraints. Thus, the size of the error ellipses gives an indication of the overall relevance of the MWA5000 constraint on a parameter.

The uncertainty in  $A$  is considerably greater from the reference experiments than from contemporary CMB measurements. Table 4 clearly displays the degeneracies (as normalized covariance factors with magnitudes close to unity) between  $A$ ,  $\Omega_b$ ,  $h$ , and more unexpectedly,  $n_s$ , responsible for the weak constraint on  $A$ . The degeneracy with  $n_s$  is due to the range of scales to which the experiments are sensitive, which is primarily after the pivot point for the primordial power spectrum spectral index ( $k = 0.05 \text{ Mpc}^{-1}$ ). Therefore, changes in  $n_s$  tend to appear slightly less similar to tilting to the power spectrum and more like changing the amplitude, although  $n_s$  remains well constrained. Additionally, the covariance between  $A$  and  $\Omega_b$  confirms that the baryon acoustic oscillations in the power spectrum are not contributing much information about the baryon density relative to the amplitude changes from the  $C_{Jy}$  and Jacobian factors. Despite the weak constraints on  $A$ ,  $\Omega_b$ , and  $h$ , the MWA5000 may be well suited to contribute to knowledge of  $\Omega_M$  and the primordial power spectrum through  $n_s$  and  $s$ .

Finally, the constraints on the amplitudes of the residual astrophysical foreground and residual thermal offset terms are especially encouraging. Neither contribution is significantly degenerate with changes to the neutral hydrogen power spectrum. In particular, the long, diminishing tail of the neutral hydrogen power spectrum provides many statistical samples which contribute little to knowledge of the cosmological parameters, yet provide good references to prevent degeneracy with changes in the magnitude of the residual thermal offset. Thus,  $P_N$  is constrained to better than 2% of the peak value of  $P_{HI}$  for the MWA and 0.01% for the MWA5000. The residual astrophysical foreground term is more somewhat more complicated and discussed in detail below.

##### 4.1. Residual Foreground Contamination

Mitigating astrophysical foreground contamination is an important issue for low-frequency EOR experiments, whether

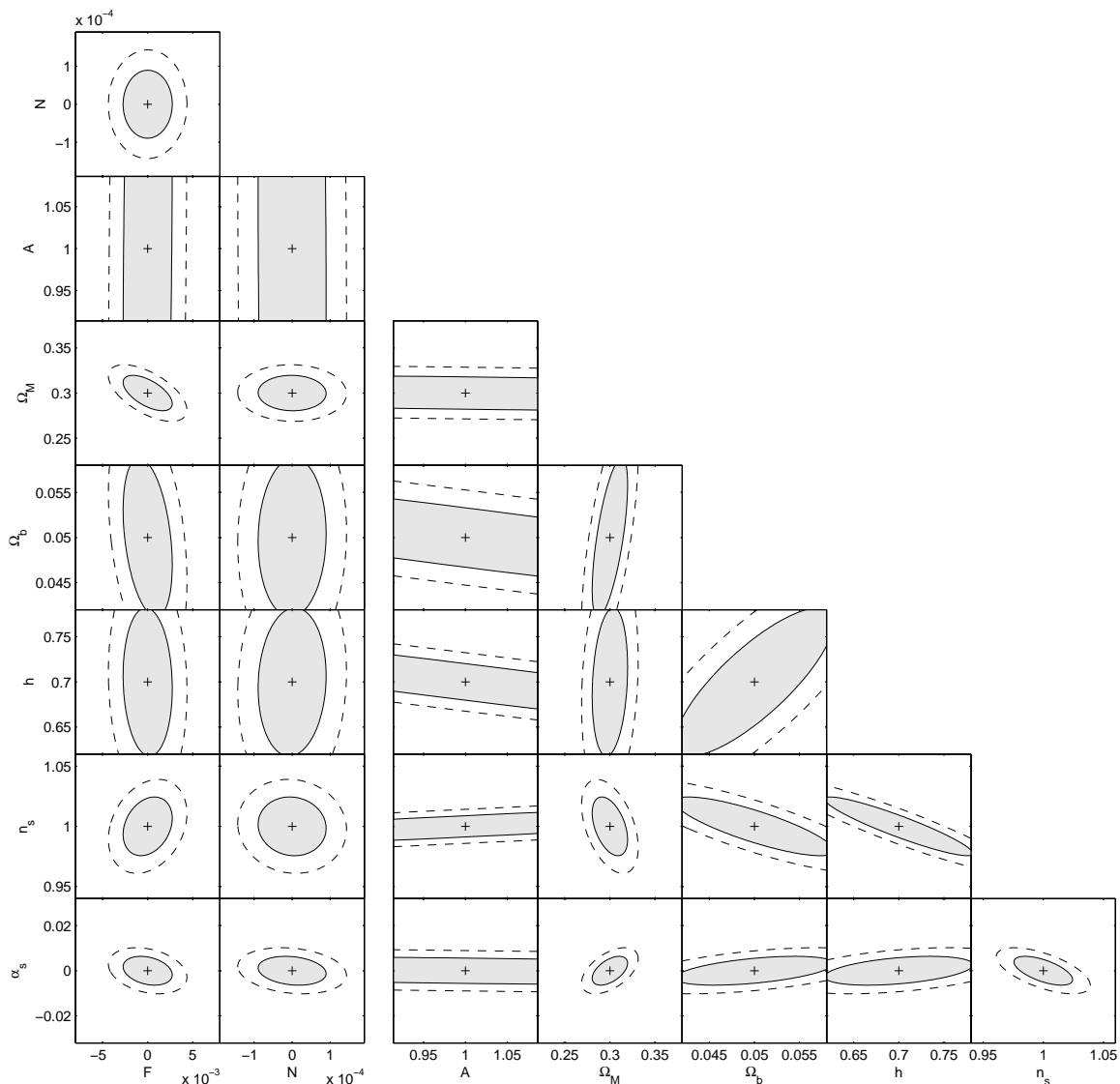


FIG. 2.— Marginalized elliptical error regions for pairs of model parameters for the baseline MWA5000 observation. The contours are for 68% (solid) and 95% (dashed) likelihood. The first two columns are for combinations with the parameters describing the magnitudes of residual astrophysical foreground contamination and the residual thermal offset. The remaining five columns are for the cosmological parameters. The bounds of the plotted regions for the cosmological parameters are set at twice the uncertainties ( $\sim 2\sigma$ ) reported in the WMAP first-year results for the respective parameters. Thus, if the dotted ellipse is visible in a particular plot, the constraints on the parameters would be an improvement over WMAP. It is evident that the MWA5000 would do a relatively good job of constraining  $\Omega_M$ ,  $n_s$ , and  $\alpha_s$ , and a comparatively poor job of constraining  $\Omega_b$  and  $h$ . The inability of the MWA5000 to constrain the scalar amplitude,  $A$ , of the power spectrum is due to degeneracies with other parameters, in particular  $\Omega_b$  and  $h$ , but also  $n_s$ .

attempting to constrain cosmological models or determine reionization processes and scenarios. To this end, the relationships between  $P_{HI}$ ,  $P_F$ , and  $P_N$ , as described by the covariance between our model parameters  $A$ ,  $F$ , and  $N$  are very useful to study in some detail.

As discussed in Sections 2 and 3, the residual foreground contamination is expected to be a power-law along the line-of-sight direction and to have little structure in the transverse directions. This is distinct from the 21 cm power spectrum with its generally spherical symmetry. Therefore, the residual foregrounds should be well separated from the cosmological models.

However, two geometrical effects due to the shape of the observed data cylinder work to negate this distinction. First, the data cylinder is highly elongated (in  $k$ -space) along the

line-of-sight direction. For the MWA, the maximum  $k$  in the sky plane is approximately  $0.05 \text{ Mpc}^{-1}$ , while along the line-of-sight it is over  $10 \text{ Mpc}^{-1}$ . Therefore, most of the information about the 21 cm power spectrum is actually coming from the line-of-sight direction. Second, the bandwidth available for the experiments is too small to probe large scales in the line-of-sight direction and, thus, the peak of the power spectrum (at  $k \approx 0.01$ ) is not well constrained. This means that not only is most of the information coming from the line-of-sight direction, it is coming from the power law-like tail ( $\propto k^{-3}$ ) of the power spectrum. These effects combine to make the 21 cm contribution and residual foreground contamination less distinguishable in the measured power spectrum.

Fortunately, the analysis indicates that the residual foreground component is well separated from the neutral hydro-

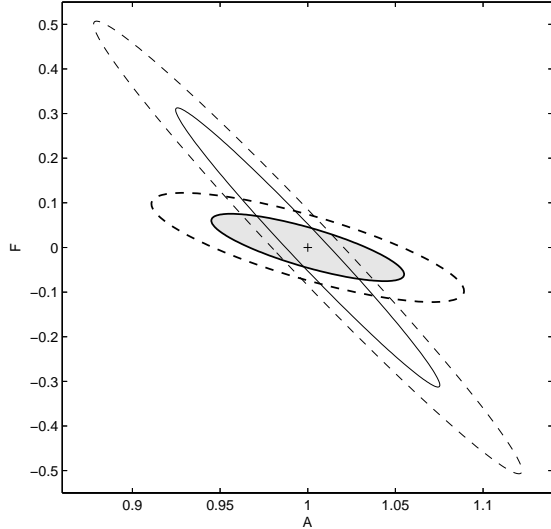


FIG. 3.— The unmarginalized error ellipses for the neutral hydrogen and residual foreground amplitude parameters,  $A$  and  $F$ , forecasted for the MWA. The thick curves are for a Fisher matrix calculation utilizing the full three-dimensional measured power spectrum, while the thin curves are for the same calculation using spherical bins in  $k$ -space. The contours are for 68% and 95% likelihood. The behavior is similar for the MWA5000, although the magnitudes are smaller.

gen power spectrum and does not affect substantially the ability to constrain the cosmological parameters. From Table 4 and Figure 2, we see that the largest degeneracy is between  $F$  and  $M$ . However, removing  $P_F$  from the model power spectrum, and thus  $F$  from the parameter set such that  $p = \{A, M, b, h, n_s, s, N\}$ , would only reduce the forecasted uncertainty on  $M$  by less than 0.003. The contributions from the residual thermal offset,  $P_N$ , are even less.

In our analysis so far we have treated the full three-dimensional measured power spectrum. This has maximized the effects of the symmetry differences between the 21 cm power spectrum and residual foreground power spectrum. We might have instead considered a reduced one-dimensional power spectrum produced by averaging over spherical bins in  $k$ -space. This approach is used commonly to reduce data in which the expected signal has approximately spherical symmetry. Such a method cannot utilize fully the symmetry differences between the 21 cm neutral hydrogen power spectrum and the residual foreground contribution.

In Figure 3, we compare the full three-dimensional treatment with the spherically-binned approach by plotting unmarginalized error ellipses in the  $A$ - $F$  plane of parameter space for both cases. It is clear that the binned method produces a significantly larger degeneracy between the magnitude of residual foreground contribution and the amplitude of the 21 cm neutral hydrogen power spectrum than the full three-dimensional treatment. While the binned method would

be a reasonable approach if only the 21 cm power spectrum were involved, it is not effective when power spectrum components with non-radial symmetries must be considered.

#### 4.2. Dark Energy Equation of State

Determining the nature of dark energy has become an important goal in astrophysics. The applicability of future large-scale structure surveys to this topic has been considered recently with generally favorable results (Seo & Eisenstein 2003; Linder 2003; Hu & Haiman 2003; Wang et al. 2004; Abdalla & Rawlings 2005). With their similarities to large-scale structure surveys, would measurements of the redshifted 21 cm neutral hydrogen power spectrum also improve knowledge of dark energy?

Including the dark energy equation of state parameter,  $w$ , as a free variable in the Fisher matrix analysis, so that  $p = \{A, M, b, h, n_s, s, w, F, N\}$ , yields little information about the nature of dark energy. Neither the MWA nor the MWA5000 are able to provide meaningful constraints on  $w$  without priors from other experiments. Furthermore, the constraints on  $M$ ,  $b$ , and  $h$  are significantly weakened (by up to an order of magnitude), although information is retained about the primordial power spectrum.

These results are not surprising. Although the MWA5000 reference experiment would be able to detect the baryon acoustic oscillations (see Figure 1), the experiment targets emission from high redshifts prior to the epoch of dark energy domination. The value of the experiment would be relevant only as an intermediate measurement between the CMB and low redshift large-scale structure surveys (Barkana 2006), but would be important if dark energy had unusual behavior at high redshifts.

#### 5. CONCLUSION

The first generations of EOR experiments have been previously shown to have the potential to characterize the processes and history of reionization at redshifts  $6 < z < 12$ . In this effort, we have considered a scenario in which reionization is not the dominant contribution to the measured power spectrum during this period, and demonstrated that the experiments would be able to contribute to knowledge of the underlying cosmology. In particular, the primordial power spectral index parameters are well constrained.

We have also considered the covariance between the neutral hydrogen power spectrum and the predicted residual foregrounds of low-frequency radio observations. The signal and contamination components were easily distinguished in the full three-dimensional power spectrum analysis.

We would like to thank Matt McQuinn, Matias Zaldarriaga, Oliver Zahn, and Lloyd Knox for fruitful discussions. Support for this work was provided by NSF grant AST-0121164 and the MIT School of Science.

#### REFERENCES

- Abdalla, F. B., & Rawlings, S. 2005, MNRAS, 360, 27  
 Alcock, C., & Paczynski, B. 1979, Nature, 281, 358  
 Ali, S. S., Bharadwaj, S., & Pandey, B. 2005, MNRAS, 363, 251  
 Barkana, R. 2006, MNRAS, submitted  
 Barkana, R., & Loeb, A. 2005a, ApJ, 624, L65  
 Barkana, R., & Loeb, A. 2005b, ApJ, 626, 1  
 Bharadwaj, S., & Ali, S. S. 2005, MNRAS, 356, 1519  
 Bond, J. R., Efstathiou, G., & Tegmark, M. 1997, MNRAS, 291, L33  
 Bowman, J. D., Morales, M. F., & Hewitt, J. N. 2006, ApJ, in press  
 Cole, S., et al. 2005, MNRAS, 362, 505  
 Di Matteo, T., Ciardi, B., & Miniati, F. 2004, MNRAS, 355, 1053  
 Feldman, H. A., Kaiser, N., & Peacock, J. A. 1994, ApJ, 426, 23  
 Hogan, C. J., & Rees, M. J. 1979, MNRAS, 188, 791  
 Hu, W., & Haiman, Z. 2003, Phys. Rev. D, 68, 063004  
 Jungman, G., Kamionkowski, M., Kosowsky, A., & Spergel, D. N. 1996, Phys. Rev. D, 54, 1332

TABLE 2  
FORECASTED UNCERTAINTIES FOR THE MODEL PARAMETERS

	A	F	D	$M$	$b$	h	$n_s$	$s$
	1.00	0.00	0.00	0.30	0.05	0.70	1.00	0.00
MWA	6.69	0.09	2e-3	0.21	0.07	0.88	0.2	0.04
MWA5000	0.45	2e-3	1e-4	0.01	6e-3	0.05	0.02	4e-3
WMAP	0.09	—	—	0.04	4e-3	0.04	0.03	0.02
SDSS	0.10	—	—	0.05	2e-3	0.04	0.03	—

NOTE. — Forecasted 1- $\sigma$  uncertainties for the model parameters. The first row gives the fiducial values for reference. The MWA reference experiment does not significantly constrain cosmological parameters, while the MWA5000 does a reasonably good job, particularly for  $M$  and the primordial power spectrum spectral index descriptors,  $n_s$  and  $s$ . For comparison, the last two rows display approximate constraints for similar models from WMAP (Spergel et al. 2003, Their Table 10) and SDSS (Tegmark et al. 2004b, Their Table 3).

TABLE 3  
COVARIANCE MATRIX FOR MWA

	A	F	D	$M$	$b$	h	$n_s$	$s$
A	1.00							
F	-0.09	1.00						
D	-0.09	0.01	1.00					
$M$	-0.04	-0.72	-0.04	1.00				
$b$	-0.87	-0.24	0.04	0.49	1.00			
h	-0.97	0.24	0.11	-0.20	0.72	1.00		
$n_s$	0.95	0.04	-0.15	-0.12	-0.82	-0.92	1.00	
$s$	-0.41	-0.37	-0.15	0.63	0.69	0.23	-0.32	1.00

NOTE. — Elements of the covariance matrix for the MWA calculated by taking the inverse of the Fisher matrix,  $F$ . Each element has been normalized according to  $c_{ab} = \frac{F_{ab}}{c_{aa}c_{bb}}$ , where the diagonal elements are the squares of the 1- $\sigma$  uncertainties given in Table 2.

TABLE 4  
COVARIANCE MATRIX FOR MWA5000

	A	F	D	$M$	$b$	h	$n_s$	$s$
A	1.00							
F	0.20	1.00						
D	-0.07	0.00	1.00					
$M$	-0.40	-0.60	-0.02	1.00				
$b$	-0.93	-0.35	0.05	0.66	1.00			
h	-0.97	-0.08	0.08	0.19	0.81	1.00		
$n_s$	0.93	0.27	-0.07	-0.46	-0.83	-0.92	1.00	
$s$	-0.48	-0.28	-0.20	0.53	0.50	0.42	-0.62	1.00

NOTE. — Same as Table 3, but for the MWA5000.

- Knox, L. 1995, Phys. Rev. D, 52, 4307  
Linder, E. V. 2003, Phys. Rev. D, 68, 083504  
Loeb, A., & Zaldarriaga, M. 2004, Physical Review Letters, 92, 211301  
McQuinn, M., Zahn, O., Zaldarriaga, Z., Hernquist, L., & Furlanetto, S. 2006, ApJ, submitted  
Morales, M. F. 2005, ApJ, 619, 678  
Morales, M. F., Bowman, J. D., & Hewitt, J. N. 2006, ApJ, submitted  
Morales, M. F., & Hewitt, J. 2004, ApJ, 615, 7  
Percival, W. J., et al. 2001, MNRAS, 327, 1297  
Santos, M. G., Cooray, A., & Knox, L. 2005, ApJ, 625, 575  
Scott, D., & Rees, M. J. 1990, MNRAS, 247, 510  
Seljak, U., & Zaldarriaga, M. 1996, ApJ, 469, 437  
Seo, H.-J., & Eisenstein, D. J. 2003, ApJ, 598, 720  
Shapiro, P. R., Giroux, M. L., & Babul, A. 1994, ApJ, 427, 25  
Spergel, D. N., et al. 2003, ApJS, 148, 175  
Sunyaev, R. A., & Zeldovich, Y. B. 1972, A&A, 20, 189  
Tegmark, M., et al. 2004a, ApJ, 606, 702  
Tegmark, M., Hamilton, A. J. S., Strauss, M. A., Vogeley, M. S., & Szalay, A. S. 1998, ApJ, 499, 555  
Tegmark, M., et al. 2004b, Phys. Rev. D, 69, 103501  
Tegmark, M., Taylor, A. N., & Heavens, A. F. 1997, ApJ, 480, 22  
Verde, L., et al. 2003, ApJS, 148, 195  
Wang, S., Khoury, J., Haiman, Z., & May, M. 2004, Phys. Rev. D, 70, 123008  
Wang, X., Tegmark, M., Santos, M., & Knox, L. 2006, Phys. Rev. D, submitted  
Zaldarriaga, M., Furlanetto, S. R., & Hernquist, L. 2004, ApJ, 608, 622  
Zaldarriaga, M., Spergel, D. N., & Seljak, U. 1997, ApJ, 488, 1